Journal of Geodesy (1999) 73: 10–22

Journal of Geodesy

An analysis of vertical deflections derived from high-degree spherical harmonic models

C. Jekeli

Department of Civil and Environmental Engineering and Geodetic Science, The Ohio State University, 2070 Neil Ave, Columbus, OH 43210, USA
e-mail: jekeli.1@osu.edu; Tel.: +1 614 292 7117; Fax: +1 614 292 2957

Received: 9 December 1997 / Accepted: 21 August 1998

Abstract. The theoretical differences between the Helmert deflection of the vertical and that computed from a truncated spherical harmonic series of the gravity field, aside from the limited spectral content in the latter, include the curvature of the normal plumb line, the permanent tidal effect, and datum origin and orientation offsets. A numerical comparison between deflections derived from spherical harmonic model EGM96 and astronomic deflections in the conterminous United States (CONUS) shows that correcting these systematic effects reduces the mean differences in some areas. Overall, the mean difference in CONUS is reduced from −0.219 arcsec to −0.058 arcsec for the south–north deflection, and from +0.016 arcsec to +0.004 arcsec for the west–east deflection. Further analysis of the root-mean-square differences indicates that the high-degree spectrum of the EGM96 model has significantly less power than implied by the deflection data.

Key words. Deflection of the vertical · Spherical harmonic model · Normal plumb-line curvature

1 Introduction

High-degree spherical harmonic models of the Earth's geopotential, whose development is motivated primarily by needs for accurate global geoid modeling, may also be used to compute other quantities, such as the deflection of the vertical. The amplification of errors in such computations coming from inaccurate high-degree coefficients will not be considered here; this may be studied independently in the context of "ill-posed" problems. On the other hand, such gravimetric deflections differ not only quantitatively, but also in definition, from geometric deflections of the vertical. Aside from the obvious limited resolution imposed by the degree of truncation, vertical deflections from spherical harmonic models differ, in principle, from their geometric counterpart mostly because of the curvature of the normal plumb line. This is a systematic effect that is usually small, but may be significant at very high flight altitudes: for example, if the spherical harmonic models are used to compensate inertial navigation systems (INS) for the effects of gravitation. A rigorous comparison is presented here that identifies this and all other differences, including the question of permanent tide effects. Subsequently, a numerical comparison between astronomical and gravimetric deflections is used to quantify these effects for the conterminous United States and to evaluate the high-degree spectrum of the EGM96 spherical harmonic model.

2 The geometric deflection of the vertical

The deflection of the vertical is an angle that describes the deviation of the true vertical, as defined by the direction of Earth's gravity vector, with respect to some reference direction. The reference direction may be defined purely geometrically or physically. The classic geometric definition of the reference direction identifies it as the perpendicular to an ellipsoid (a *geodetic datum*) that approximates the geoid, either locally or globally.

Alternatively, the reference direction may be associated with the direction of a gravity vector belonging to some reference (or *normal*) gravity field; this is the physical definition. The normal gravity field is defined to be that field generated by an ellipsoid containing all the Earth's mass (including atmosphere) and rotating with the Earth, and such that the ellipsoid is an equipotential surface of the field thus generated. Furthermore, the ellipsoid should be a best approximation of the geoid and should have its center at the Earth's center of mass.

The geometric ellipsoid (geodetic datum) and the ellipsoid of the reference gravity field may be identical.

However, in general, they differ in any or all of the following: size, shape, location, and orientation. In that case, standard formulas exist to transform deflections of the vertical from one to the other geometric reference directions (see e.g. Heiskanen and Moritz 1967, p. 207; Rapp 1992, p. 85).

The definitions of the deflection of the vertical are described in the following paragraphs (Torge 1991; see also Fig. 1). The *Helmert* definition is perhaps the most common and corresponds to the classic geometric definition alluded to above. According to this definition, the vertical deflection is the angle at a point, P, between the gravity vector that, extended upward, defines the astronomic zenith, and a straight line that passes through the point, P, and is normal to the reference ellipsoid; this line defines the geodetic zenith. In terms of south–north, ξ, and west–east, η, components of the deflection, one has (Pick et al. 1973, p. 432)

$$\begin{aligned}\xi &= \Phi - \phi + \frac{1}{2}\eta^2 \tan\phi + \text{3rd order terms}\\ \eta &= (\Lambda - \lambda)\cos\phi + \text{3rd order terms}\end{aligned} \tag{1}$$

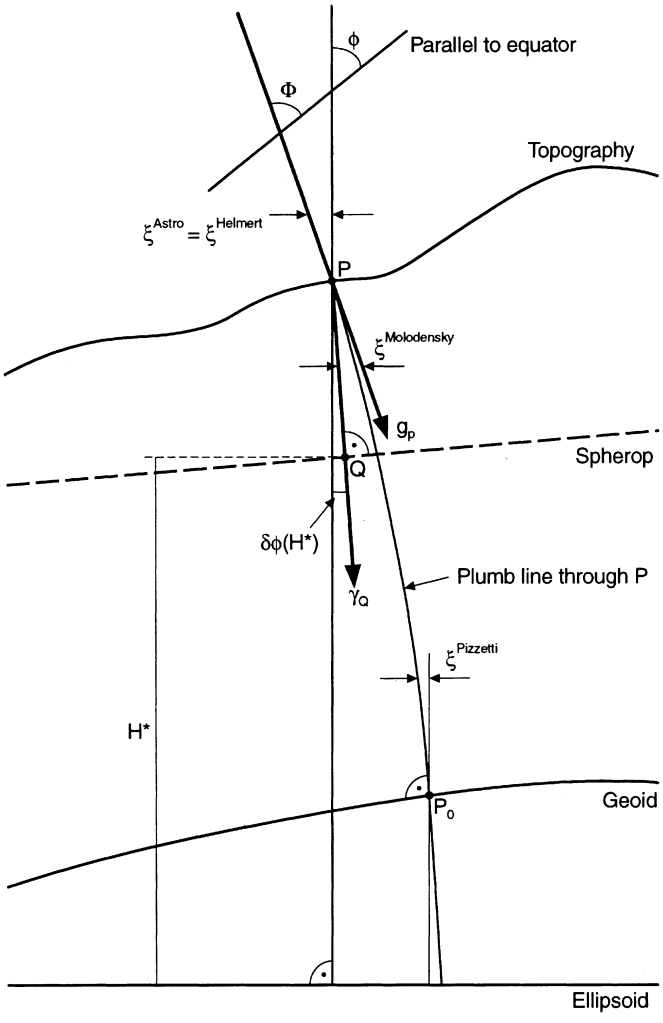

Fig. 1. Relationships between different deflections of the vertical (ξ component)

where (Φ, Λ) are astronomic coordinates (latitude and longitude) of the point and (ϕ, λ) are the corresponding geodetic coordinates. In Eq. (1), it is assumed that the north poles of the astronomic and geodetic coordinate systems coincide.

The deflection components are small angles, on the order of several arcseconds; and the higher-order terms in Eq. (1) refer to terms proportional to powers of the deflection components. Neglecting the second- and higher-order terms, the definitions of Eq. (1) conform also to the astronomically determined deflection, redesignated as

$$\begin{aligned}&\xi^{\text{astro}} = \Phi - \phi; \quad \eta^{\text{astro}} = (\Lambda - \lambda)\cos\phi;\\ &\boldsymbol{\Theta}^{\text{astro}} = (\xi^{\text{astro}}, \eta^{\text{astro}})^{\mathrm{T}}\end{aligned} \tag{2}$$

where $\boldsymbol{\Theta}^{\text{astro}}$ is a two-component vector whose magnitude is the total deflection angle (to first-order approximation). The Helmert, or astronomic, deflection of the vertical is the deflection that, when scaled by the magnitude of gravity, is required in the inertial navigation equations for horizontal positions and velocities (Britting 1971). It represents the horizontal component of the gravity vector with respect to the local vertical in the navigation frame, which is aligned with the ellipsoidal normal.

Another definition is named after Pizzetti, who prescribed the deflection of the vertical as the angle between the gravity vector at a point on the *geoid* and the perpendicular to the ellipsoid. (The Helmert deflection at a point on the geoid is also the Pizzetti deflection.) Pizzetti's definition may be extended to points above the geoid according to Molodensky's definition of the deflection as the angle at a point, P, between the gravity vector at P and the normal gravity vector at the conjugate point, Q. This point, Q, is the intersection of a spheropotential surface (spherop) with its normal through P, where the normal potential of this spherop equals the actual gravity potential at P.

The difference between the Helmert and Molodensky deflections at a point is due to the curvature of the normal plumb line. This effect occurs only in the south–north component and is given to first order by (Heiskanen and Moritz 1967, p. 196)

$$\delta\xi_{\text{norm.curv}}(h) = -\delta\phi_{\text{norm.curv}}(h) \approx 0.17\, h_{\text{km}} \sin 2\phi[\text{arcsec}] \tag{3}$$

where h_{km} is the normal height in units of km. This effect on the deflection is in the positive sense as a consequence of the convergence from equator to pole of the equipotential surfaces (spherops) of the normal gravity field. With reference to Fig. 1, the following relationship holds:

$$\xi^{\text{astro}} \equiv \xi^{\text{Helmert}} = \xi^{\text{Molodensky}} + \delta\xi_{\text{norm.curv}} \tag{4}$$

Clearly, the effect of the normal curvature increases with altitude of the point. Usually it is of little concern in low-elevation terrain; however, the correction can become

significant at high altitudes, e.g. those navigated by an INS.

The difference between the Helmert (or also Molodensky) and Pizzetti deflections has to do with the fact that the point of definition is different and subsequently the actual gravity vector directions are different (curvature of *actual* plumb line). Thus, these differences are due to the local non-parallelism of the equipotential surfaces of the actual gravity field. The Pizzetti definition is of no further concern here.

3 The gravimetric deflection of the vertical

The deflection of the vertical (specifically, Molodensky's version) can be determined from gravimetric data, at least under certain approximations. When thus determined, it is given the special name *gravimetric* deflection of the vertical. Using the geometry of the gravity vectors, the Molodensky deflection components, along south–north and west–east directions, are given in a local north-west-up (NWU) coordinate system (again, neglecting non-linear terms) by

$$\begin{aligned}\xi^{\text{Molodensky}}(P) &\approx \frac{-1}{g_P}g_\phi(P) - \frac{-1}{\gamma_Q}\gamma_\phi(Q)\\ &= -\frac{1}{\gamma_Q}\big(g_\phi(P) - \gamma_\phi(Q)\big) - \delta\xi_g\\ \eta^{\text{Molodensky}}(P) &\approx \frac{-1}{g_P}g_\lambda(P) - \frac{-1}{\gamma_Q}\gamma_\lambda(Q)\\ &= -\frac{1}{\gamma_Q}(g_\lambda(P) - \gamma_\lambda(Q)) - \delta\eta_g\end{aligned} \tag{5}$$

where g_ϕ and g_λ are horizontal components of the gravity vector at P, and γ_ϕ and γ_λ ($\gamma_\lambda = 0$!) are horizontal components of the normal gravity vector at Q, all in the local NWU coordinate system aligned with the ellipsoid normal through P. The quantities $\delta\xi_g$ and $\delta\eta_g$ are small effects due to approximating the divisor g_P by γ_Q, and are given by

$$\begin{aligned}\delta\xi_g &= \frac{g_\phi(P)}{g_P}\frac{\gamma_Q - g_P}{\gamma_Q} \approx \xi_P\frac{\Delta g_P}{\gamma_Q}\\ \delta\eta_g &= \frac{g_\lambda(P)}{g_P}\frac{\gamma_Q - g_P}{\gamma_Q} \approx \eta_P\frac{\Delta g_P}{\gamma_Q}\end{aligned} \tag{6}$$

where Δg_P is the gravity anomaly.

The linear approximation in Eq. (5) is practically the same as for the astronomic deflection, where the only difference is due to the normal curvature that displaces the normal zenith from the geodetic zenith; this is inconsequential in the second-order term in Eq. (1).

Consider the disturbing potential, T, which is given by

$$T = W - U \tag{7}$$

where W is the actual gravity potential and U is the normal gravity potential. Then, noting that the gravity vector is the gradient of the potential, one has from Eq. (5)

$$\begin{aligned}\xi^{\text{Molodensky}}(P) &= -\frac{1}{\gamma_Q}\left(\left.\frac{\partial W}{(M+h)\partial\phi}\right|_P - \left.\frac{\partial U}{(M+h)\partial\phi}\right|_Q\right) - \delta\xi_g\\ \eta^{\text{Molodensky}}(P) &= -\frac{1}{\gamma_Q}\left(\left.\frac{\partial W}{(N+h)\cos\phi\,\partial\lambda}\right|_P - \left.\frac{\partial U}{(N+h)\cos\phi\,\partial\lambda}\right|_Q\right) - \delta\eta_g\end{aligned} \tag{8}$$

where N and M are the principal radii of curvature of the ellipsoid and h is the ellipsoidal height of the point.

One may define the gravimetric deflection of the vertical as

$$\begin{aligned}\xi^{\text{grav}}(P) &= -\frac{1}{\gamma_Q}\left.\frac{\partial T}{(M+h)\,\partial\phi}\right|_P\\ \eta^{\text{grav}}(P) &= -\frac{1}{\gamma_Q}\left.\frac{\partial T}{(N+h)\cos\phi\,\partial\lambda}\right|_P\\ \boldsymbol{\Theta}^{\text{grav}} &= (\xi^{\text{grav}}, \eta^{\text{grav}})^{\mathrm{T}}\end{aligned} \tag{9}$$

The gravimetric deflection is obtained from the horizontal derivatives of the disturbing potential, T, at a point. By "horizontal" one means perpendicular to the ellipsoid normal that passes through the point. The Molodensky deflections, Eqs. (8), would equal the gravimetric deflections, Eqs. (9), by ignoring the small terms, $\delta\xi_g$ and $\delta\eta_g$, and by assuming that the normal gravity vectors at P and Q are parallel, i.e. by neglecting the curvature of the normal plumb line between P and Q. Thus

$$\begin{aligned}\xi^{\text{Molodensky}}(P) &= \xi^{\text{grav}}(P) + \delta\xi_{\text{norm.curv}}(\zeta_P) - \delta\xi_g\\ \eta^{\text{Molodensky}}(P) &= \eta^{\text{grav}}(P) - \delta\eta_g\end{aligned} \tag{10}$$

where ζ_P is the height anomaly at P. Equations (10) show the approximations made in determining the Molodensky deflections gravimetrically [according to Eqs. (9)].

The determination of the gravimetric deflection comes directly from a solution to the disturbing potential. There are two classic formulations of this solution in terms of a boundary-value problem, where gravimetric quantities, the gravity anomalies, constitute the boundary values. These two forms are the Stokes formula (Heiskanen and Moritz 1967; it is not considered further here) and the spherical harmonic series:

$$T(r,\theta,\lambda) = \frac{kM}{r}\sum_{n=2}^{\infty}\sum_{m=-n}^{n}\left(\frac{a}{r}\right)^n C_{n,m}\bar{Y}_{n,m}(\theta,\lambda) \tag{11}$$

where (r,θ,λ) are spherical polar coordinates, kM is the product of Newton's gravitational constant and the Earth's total mass (including atmosphere), a is the

equatorial radius of the reference ellipsoid, and the functions $\bar{Y}_{n,m}$ are spherical harmonic functions fully normalized such that the coefficients $C_{n,m}$ are given by

$$C_{n,m} = \frac{a^2}{4\pi kM(n-1)} \iint_\sigma \Delta g(\theta,\lambda)\bar{Y}_{n,m}(\theta,\lambda)\,\mathrm{d}\sigma \tag{12}$$

The zero-degree term $(n = 0)$ is missing in Eq. (11) under the assumptions that the normal ellipsoid contains the mass, M, and that the geopotential on the geoid and the normal potential on the ellipsoid are equal. [These assumptions are immaterial for the gravimetric deflections of the vertical, Eq. (9), since they affect only the *constant* bias of T.] The first-degree $(n = 1)$ terms are omitted under the assumption that the coordinate system is geocentric.

Equation (12) for the coefficients $C_{n,m}$ represents an idealization, being in the first place a spherical approximation, where the gravity anomaly is related in spherical approximation to the disturbing potential. Modern spherical harmonic models are constructed with great care to correct for these and other approximations (Rapp and Pavlis 1990). Therefore, one may take Eq. (11) to be devoid of all such approximations to the extent possible using the available data, and assume that the set of spherical harmonic coefficients $\{C_{n,m}\}$ has been correspondingly corrected. Equation (11) thus represents the *true* disturbing potential outside a sphere enclosing all terrestrial masses, where the atmosphere and all extraterrestrial masses are assumed removed. That is, the disturbing potential of Eq. (11) is given in the *non-tide*, or *tide-free* system. It is to be noted that the astronomic (Helmert) deflections are given in the *mean-tide* system, since tidal corrections, amounting to no more than a few hundredths of an arcsecond, are not applied (R. Anderson, NIMA, pers. comm. 1997).

4 The permanent tidal effect on deflections of the vertical

A brief review of the tidal effects is in order. The gravitational tidal potential due to an external point-mass body, designated generically as B, is given approximately by Torge (1991) as

$$\begin{aligned} V_{\mathrm{B}}(r,\psi,\lambda) = D_{\mathrm{B}}(r)\Big[& \cos^2\psi\cos^2\delta_{\mathrm{B}}\cos 2t_{\mathrm{B}} \\ & + \sin 2\psi \sin 2\delta_{\mathrm{B}}\cos t_{\mathrm{B}} \\ & + 3\left(\sin^2\psi - \frac{1}{3}\right)\left(\sin^2\delta_{\mathrm{B}} - \frac{1}{3}\right)\Big] \end{aligned} \tag{13}$$

where t_{B} is the hour angle of the body

$$t_{\mathrm{B}} = \lambda + t_{\mathrm{G}} - \alpha_{\mathrm{B}} \tag{14}$$

and $(\alpha_{\mathrm{B}}, \delta_{\mathrm{B}})$ are the right ascension and declination of the body, while t_{G} is the hour angle of the vernal equinox at the Greenwich meridian (i.e. sidereal time). The coordinates of the point of evaluation are given in terms of geocentric latitude, ψ. The radial dependence of V_{B} is given by

$$D_{\mathrm{B}}(r) = \frac{3}{4}kM_{\mathrm{B}}\frac{r^2}{r_{\mathrm{B}}^3} \tag{15}$$

where r_{B} is the mean distance between the Earth and the body. D_{B} is known as *Doodson's coefficient* and reflects that Eq. (13) is a second-degree *interior* harmonic potential.

The tidal potential, Eq. (13), varies in time, as viewed at a point on the Earth, with different periods: from fortnightly (due to the moon) or semi-annually (due to the sun) as the coordinates $(\alpha_{\mathrm{B}}, \delta_{\mathrm{B}})$ vary, to diurnally because of Earth's rotation described by t_{G}. There is also a constant part, the average over 18 years, that is not zero; this is the *permanent* tide due to the (crudely) approximate coplanarity of the Earth–sun–moon system. The sun and moon are the only extraterrestrial bodies of consequence and one may denote

$$V_{\mathrm{t}}(r,\psi,\lambda) = V_{\mathrm{sun}}(r,\psi,\lambda) + V_{\mathrm{moon}}(r,\psi,\lambda) \tag{16}$$

The components of tilt of the Earth's equipotential surface (e.g. geoid) due to the tidal potential are given by (Vanicek 1980)

$$\delta\xi_{\mathrm{t}} = -\frac{\partial V_{\mathrm{t}}}{\gamma R\partial\psi}; \quad \delta\eta_{\mathrm{t}} = -\frac{\partial V_{\mathrm{t}}}{\gamma R\cos\psi\partial\lambda} \tag{17}$$

where no distinction needs to be made between geodetic and geocentric latitude. To get an idea of the rough order of magnitude of the tidal tilt, consider that, with appropriate values for the sun's and moon's mass, Doodson's coefficient is

$$\frac{D_{\mathrm{sun}}(R) + D_{\mathrm{moon}}(R)}{\gamma R} = 0.013 \text{ arcsec} \tag{18}$$

Only the permanent tidal effect is of interest in the numerical analysis presented later. Using accurate ephemerides (admittedly, extreme accuracy is not warranted) of the sun and moon over three 18-year periods, Cartwright and Tayler (1971) analyzed the total ensuing tidal potential and arrived at amplitudes for over 500 spectral constituents, including the constant (permanent) component. Rapp (1983) used this permanent part to infer a geoid deformation given by (Heikkinen 1978 did his own analysis and obtained the same result)

$$\delta N_{\mathrm{t}}^0 = \frac{V_{\mathrm{t}}^0}{\gamma} = 0.099 - 0.296\sin^2\psi[\mathrm{m}] \tag{19}$$

The corresponding permanent tilt in the geoid is, therefore, given from Eq. (17) by

$$\begin{aligned} \delta\xi_{\mathrm{t}}^0 &= 0.0096\sin 2\psi \text{ [arcsec]} \\ \delta\eta_{\mathrm{t}}^0 &= 0 \end{aligned} \tag{20}$$

Thus, only the south–north deflection of the vertical experiences a permanent tidal deformation.

These results hold only for a rigid Earth. For the more realistic elastic model, the Earth's surface itself

deforms under the influence of the tidal forces. The deformation occurs radially as well as tangentially. Furthermore, this deformation redistributes terrestrial mass and consequently generates an additional change in gravitational potential. The tangential displacement is characterized as a ratio, ℓ, between the actual displacement and that of a perfectly nonviscous fluid Earth. If the Earth were fluid, then the horizontal displacement, expressed in terms of the tidal potential as $(1/\gamma)\partial V_t/\partial\psi$, would cause a change in the direction of the perpendicular to the surface (equipotential, in this case) given by $((1/\gamma)\partial V_t/\partial\psi)/R$. The Earth is not fluid and this is expressed by the ratio, ℓ, so that the horizontal displacement is actually $(\ell/\gamma)\partial V_t/\partial\psi$, and the change in direction of the perpendicular is $((\ell/\gamma)\partial V_t/\partial\psi)/R$.

The deformation changes the gravitational potential by a fraction of the tidal potential due to the mass redistribution, so that for the deformed Earth the total change in potential is $(1+k)V_t$. The unitless numbers k and ℓ are named after A.E.H. Love (*Love* numbers) and have observed values (Lambeck 1988) of $k = 0.29$, $\ell = 0.08$. The total tidal effect on the (south–north) deflection is therefore

$$\delta\xi_{td} = -(1+k)\frac{\partial V_t}{\gamma R\partial\psi} + \ell\frac{\partial V_t}{\gamma R\partial\psi} \tag{21}$$

and the permanent tilt is modified to

$$\begin{aligned}\delta\xi^0_{td} &= 0.012\sin 2\psi \text{ [arcsec]}\\ \delta\eta^0_{td} &= 0\end{aligned} \tag{22}$$

The following relationship holds:

$$\xi^{grav}_{\text{mean tide}} = \xi^{grav}_{\text{tide-free}} + \delta\xi^0_{td} \tag{23}$$

That is, the deflection becomes more positive with a further flattening of the equipotential surfaces due to the tidal attraction.

5 Practical differences between gravimetric and helmert deflections

A finite set of computed spherical harmonic coefficients constitutes a *model* for the disturbing potential in free space, meaning that the series of Eq. (11) is truncated at some degree, n_{max}. In addition, a particular model has errors associated with the uncertainties of the computed coefficients, which, in turn, arise from data measurement uncertainties and errors due to unaccounted approximations. The errors due to measurement uncertainty may be characterized statistically by a variance/covariance matrix for the coefficients; other errors can be quantified to some extent in terms of upper bounds. Rarely, however, are detailed and accurate error statistics obtainable for the entire set of coefficients, due to limitations in computer power and knowledge about the actual statistics or characteristics of the data errors. This is especially true for the higher-degree parts of the model, whereas it is computationally tractable to determine the low-degree error statistics using rigorous least-squares adjustments of satellite orbit perturbation observations. High-degree statistics of the model usually comprise a set of estimated standard deviations for the coefficients.

Let the computed coefficients be denoted by $\{\hat{C}_{n,m}\}$; then the model for the disturbing potential is given by

$$\hat{T}(r,\theta,\lambda) = \frac{kM}{r}\sum_{n=2}^{n_{max}}\sum_{m=-n}^{n}\left(\frac{a}{r}\right)^n\hat{C}_{n,m}\bar{Y}_{n,m}(\theta,\lambda) \tag{24}$$

The gravimetric deflections of the vertical are then obtained by differentiation according to Eq. (9)

$$\begin{Bmatrix}\hat{\xi}^{grav}(r,\theta,\lambda)\\ \hat{\eta}^{grav}(r,\theta,\lambda)\end{Bmatrix} = -\frac{1}{\gamma}\frac{kM}{r^2}\sum_{n=2}^{n_{max}}\sum_{m=-n}^{n}\left(\frac{a}{r}\right)^n\hat{C}_{n,m} \times\begin{Bmatrix}-\frac{\partial}{\partial\theta}\\ \frac{\partial}{\sin\theta\,\partial\lambda}\end{Bmatrix}(\bar{Y}_{n,m}(\theta,\lambda)) \tag{25}$$

where a further spherical approximation is made in the direction of the derivative, being orthogonal to the radius from the origin, rather than the normal to the ellipsoid. The effect of this approximation applies only to the south–north component and can be evaluated using the equation (see Fig. 2)

$$\begin{aligned}\frac{\partial}{(M+h)\partial\phi} &= -\cos v\frac{\partial}{r\partial\theta} - \sin v\frac{\partial}{\partial r}\\ &\approx -\frac{\partial}{r\,\partial\theta} - v\frac{\partial}{\partial r}\end{aligned} \tag{26}$$

where v is the angle between the meridian radius of curvature and the spherical radius

$$v = \phi - \psi \approx f(1-\tfrac{1}{2}f)\sin 2\phi \tag{27}$$

f is the flattening of the ellipsoid. The longitudinal derivative is unaffected, because

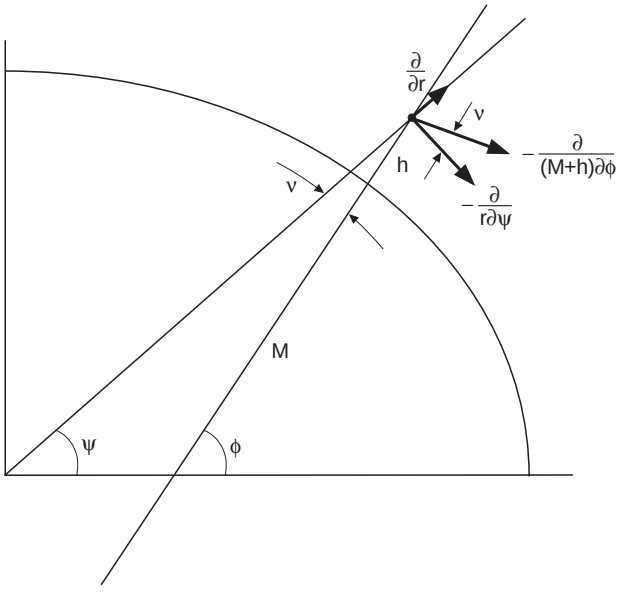

Fig. 2. Partial derivatives along different horizons

$$\frac{\partial}{(N+h)\cos\phi\,\partial\lambda} = \frac{\partial}{r\sin\theta\,\partial\lambda} \tag{28}$$

Thus, we have the following error terms:

$$\begin{aligned}\hat{\xi}^{\text{grav}}(r,\theta,\lambda) &= \xi^{\text{grav}}(r,\theta,\lambda) + \delta\xi_v + \delta\xi_{\text{trunc}} + \delta\xi_{\text{coeff.err}}\\ \hat{\eta}^{\text{grav}}(r,\theta,\lambda) &= \eta^{\text{grav}}(r,\theta,\lambda) + \delta\eta_{\text{trunc}} + \delta\eta_{\text{coeff.err}}\end{aligned} \tag{29}$$

where, from Eq. (26) and with the definition of gravity disturbance, δg, the derivative error is

$$\delta\xi_v = v\frac{\delta g_{\text{P}}}{\gamma_Q} \tag{30}$$

The truncation error of Eq. (25) is given by

$$\begin{Bmatrix}\delta\xi_{\text{trunc}}\\ \delta\eta_{\text{trunc}}\end{Bmatrix} = \frac{1}{\gamma}\frac{kM}{r^2}\sum_{n=n_{\max}+1}^{\infty}\sum_{m=-n}^{n}\left(\frac{a}{r}\right)^n C_{n,m} \times \begin{Bmatrix}-\frac{\partial}{\partial\theta}\\ \frac{\partial}{\sin\theta\,\partial\lambda}\end{Bmatrix}(\bar{Y}_{n,m}(\theta,\lambda)) \tag{31}$$

and the error due to harmonic coefficient error is

$$\begin{Bmatrix}\delta\xi_{\text{coeff.err}}\\ \delta\eta_{\text{coeff.err}}\end{Bmatrix} = -\frac{1}{\gamma}\frac{kM}{r^2}\sum_{n=2}^{n_{\max}}\sum_{m=-n}^{n}\left(\frac{a}{r}\right)^n \delta C_{n,m} \times \begin{Bmatrix}-\frac{\partial}{\partial\theta}\\ \frac{\partial}{\sin\theta\,\partial\lambda}\end{Bmatrix}(\bar{Y}_{n,m}(\theta,\lambda)) \tag{32}$$

Note that if the coordinates of the point of evaluation are given as geodetic coordinates (h,ϕ,λ) then these must be transformed to geocentric coordinates (r,θ,λ) before evaluating Eq. (25). Also, the normal gravity γ in Eq. (25) should be evaluated at the point of computation; replacing it with the approximation kM/r^2 introduces a potentially significant error of up to 1 part in 500 of the deflection.

Other differences between gravimetric and astronomic deflections of the vertical include the offset of the center of mass from the ellipsoid center and the nonparallelism of the coordinate axes. In particular, if there is a small translation $(\Delta x,\Delta y,\Delta z)$ at the geocenter between datums, then

$$\begin{aligned}\delta\xi_{\text{trans}} &= \sin\phi\cos\lambda\frac{\Delta x}{M+h} + \sin\phi\sin\lambda\frac{\Delta y}{M+h} - \cos\phi\frac{\Delta z}{M+h}\\ \delta\eta_{\text{trans}} &= \sin\lambda\frac{\Delta x}{N+h} - \cos\lambda\frac{\Delta y}{N+h}\end{aligned} \tag{33}$$

Orientation differences, as represented by small rotation angles $(\omega_x,\omega_y,\omega_z)$ with the pivot point being the geocenter, cause deflection changes given by

$$\begin{aligned}\delta\xi_{\text{rot}} &= \sin\lambda\,\omega_x - \cos\lambda\,\omega_y\\ \delta\eta_{\text{rot}} &= -\sin\phi\cos\lambda\,\omega_x - \sin\phi\sin\lambda\,\omega_y + \cos\phi\,\omega_z\end{aligned} \tag{34}$$

In Eqs. (33) and (34), (h,ϕ,λ) are the geodetic coordinates of the point of evaluation of the deflection components. It is noted that orientation differences may be due to misalignments of astronomic as well as geodetic reference systems.

6 Recapitulation

Combining Eqs. (4), (10), (23), (29), (33) and (34), we have the following relationship between the Helmert deflection and the gravimetric deflection as computed from a spherical harmonic model of the disturbing potential:

$$\begin{aligned}\hat{\xi}^{\text{astro}}(P) &= \hat{\xi}^{\text{grav}}_{\text{tide-free}}(P) + \delta\xi^0_{\text{td}} + \delta\xi_{\text{norm.curv}}(\zeta_P)\\ &\quad + \delta\xi_{\text{norm.curv}}(H^*_P) - \delta\xi_g - \delta\xi_{\text{trans}} - \delta\xi_v\\ &\quad - \delta\xi_{\text{trunc}} - \delta\xi_{\text{coeff.err}} - \delta\xi_{\text{rot}} - \delta\xi_{\text{astro.err}}\\ \hat{\eta}^{\text{astro}}(P) &= \hat{\eta}^{\text{grav}}(P) - \delta\eta_{\text{trunc}} - \delta\eta_{\text{coeff.err}} - \delta\eta_g - \delta\eta_{\text{trans}}\\ &\quad - \delta\eta_{\text{rot}} - \delta\eta_{\text{astro.err}}\end{aligned} \tag{35}$$

where the spherical harmonic model is assumed to be in the tide-free system and astronomic observation errors are also included. Missing from Eq. (35) is the periodic tidal effect on the Helmert deflection (which was not computed for the data to be analyzed in this paper), as well as the time-varying effects due to atmospheric and other mass redistributions. The constant atmospheric attraction (important for terrestrial gravity anomalies, with a maximum value of 0.87 mgal) in the horizontal direction is due to the lateral mass inhomogeneities, the largest of which results from the air being displaced by local terrain. This is about 0.05% (air–crustal density ratio) of the terrain correction for deflections and thus less than 1 milliarcsecond and negligible.

Table 1 gives an otherwise full account of the differences between the two types of deflections, Helmert and gravimetric, Eq. (25), in terms of root-mean-square (rms) values of each of the correction terms. Some of these differences are a consequence of differences in the definitions, others result from approximations to the definition. The values were obtained with $H^* = 2$ km, $\phi = 45°$, $\text{rms}(\Delta g) = 42$ mgal, $\text{rms}(\delta g) = 46$ mgal, $\text{rms}(\zeta) = 30$ m and $\text{rms}(\xi) = 5$ arcsec.

Clearly, the truncation error followed by the predicted inaccuracy in the spherical harmonic model contribute the most to the difference between the Helmert deflection and the spherical harmonic model deflection. This is not an unexpected result, since the model is limited in resolution to about 50 km, while there is significant power in the deflection signal at higher resolution. Also, the astronomic observational error associated with the Helmert deflection represents a substantial contribution. However, regionally all of these errors take on a *random* character, while the effects of next significance (numbers 1, 4, 5, 8 and 9 in Table 1) are quite *systematic*. It is noted that the normal curvature correction is definitely the most prominent of these,

Table 1. Differences between the Helmert deflection component, ζ, and the deflection as given by a truncated spherical harmonic series ($n_{\max} = 360$) [some of these also hold for η; see Eq. (35)]

Effect	Equation reference	rms value, arcsec (where appropriate)
1. Difference between Helmert and Molodensky deflection	(3)	0.34 ($h_{\mathrm{km}} = 2$)
2. Actual gravity approximated by normal gravity	(6)	0.0002
3. Difference between Molodensky and gravimetric deflection	(10)	0.005
4. Difference between mean-tide and tide-free systems	(23)	0.012
5. Horizontal derivative approximation	(30)	0.032
6. Harmonic series truncation at degree 360 (T/R[a] model)	(31)	3.7
7. Harmonic coefficient error (EGM96[b] predicted)	(32)	1.27
8. Coordinate origin differences (ITRF90[c]–WGS84)	(33)	< 0.018
9. Coordinate axes misalignment[d] (ITRF90–WGS84)	(34)	< 0.020
10. Astronomic observation error (CONUS[e])	–	0.31

[a] Tscherning/Rapp model, Tscherning and Rapp (1974).
[b] Joint NASA/NIMA Earth Gravity Model, Lemoine et al. (1996).
[c] International Terrestrial Reference Frame 1990, McCarthy (1992).
[d] Large z-axis rotation of the astronomic system (FK4 catalogue) will cause greater differences.
[e] Conterminous United States, provided by NIMA (National Imagery and Mapping Agency).

not only especially in mountainous areas, but particularly at higher flight altitudes. Certain effects can be safely neglected, for example, item numbers 2 and 3 in Table 1. Also, with the possible exception of the normal curvature correction, all other systematic effects may be neglected in the traditional reduction of geodetic quantities to the ellipsoid.

7 Numerical results

The object of this section is to compare astronomic deflections of the vertical with deflections computed from high-degree spherical harmonic models. The astronomic deflection data for the comparisons were provided by the National Imagery and Mapping Agency (NIMA, pers. commun.). The spherical harmonic models considered are the OSU91A model (Rapp et al. 1991) and the recently constructed EGM96 model (Lemoine et al. 1996). Both models are complete to degree and order $n_{\max} = 360$ and are functions of *geocentric* spherical polar coordinates (r, θ, λ). The comparison is restricted to the conterminous United States (CONUS).

The total number of astronomic deflections is 3678 and they are distributed *unevenly* across CONUS. Each astronomic deflection data record consists of two components, ξ^{astro}, η^{astro}, the orthometric height, and the *geodetic* latitude and longitude (ϕ, λ) in the WGS84 reference system. Also included is a standard deviation for each deflection component. Of the 3678 observed deflections, 117 have a combined standard deviation, $\sqrt{\sigma_\xi^2 + \sigma_\eta^2}$, that is greater than 1 arcsec. (Oddly, most of these are situated along the 35th parallel and along the eastern Florida coast.) These observed deflections were deleted from the analysis, leaving a total of 3561 deflections (Fig. 3). In this reduced set, the rms of the standard deviations for ξ^{astro} is 0.293 arcsec, and for η^{astro} it is 0.394 arcsec.

The spherical harmonic models are given in terms of spherical harmonic coefficients $\{\hat{C}_{n,m}\}$, with respect to the GRS80 normal gravity field, for all degrees and orders up to the maximum degree ($n_{\max} = 360$). Each coefficient is also associated with a given standard deviation. For the evaluation of the spherical harmonic model, Eq. (25), the orthometric height for each astronomic deflection point was added to the geoid undulation obtained from the EGM96 model in order to obtain the ellipsoidal height, h; then the geodetic coordinates (h, ϕ, λ) were converted to spherical polar coordinates (r, θ, λ). The normal gravity appearing in Eq. (25) was evaluated at the point of computation using first-order upward continuation of the normal gravity formula.

Due to the vastness and variability in terrain within CONUS, this total area was divided into six regions approximately evenly separating north from south and central from eastern and western parts (Fig. 4). These regions approximately delineate rough (west), moderate (east) and smooth (central) terrain, where further north–south distinctions may also be anticipated. In each of these areas the astronomic deflections and those implied by the spherical harmonic model may be characterized briefly by their maximum, minimum, mean and rms values, as in Table 2. The differences between the two types of deflections, both with respect to OSU91A and EGM96, are similarly characterized.

Note that $\Theta \equiv |\boldsymbol{\Theta}|$ is the magnitude of the deflection vector, and that $\Delta\Theta \equiv |\Delta\boldsymbol{\Theta}|$ represents the magnitude of the difference in deflection vectors, not the difference in magnitudes. Table 3 gives the corresponding statistics of the differences for each individual region. The rms values in these tables are computed by

$$\underset{j}{\mathrm{rms}}\,(z_j) = \sqrt{\frac{1}{N}\sum_{j=1}^{N} z_j^2}; \quad z = \xi,\ \eta,\ \Theta,\ \Delta\xi,\ \Delta\eta,\ \Delta\Theta \qquad (36)$$

where N is the number of deflections in a region.

Considering just the rms values, it is seen in Table 2 that the rms astronomic deflection is significantly larger than the rms deflection implied by either spherical harmonic model, where the discrepancy is largest in the mountainous regions. Also, the EGM96 model captures slightly more deflection information than does the

OSU91A model. This is verified by the differences between the astronomic deflections and the spherical harmonic deflections. Table 3 shows a systematic improvement, though slight, in the deflections computed by EGM96 versus OSU91A. Of particular interest are the mean differences, which could imply systematic

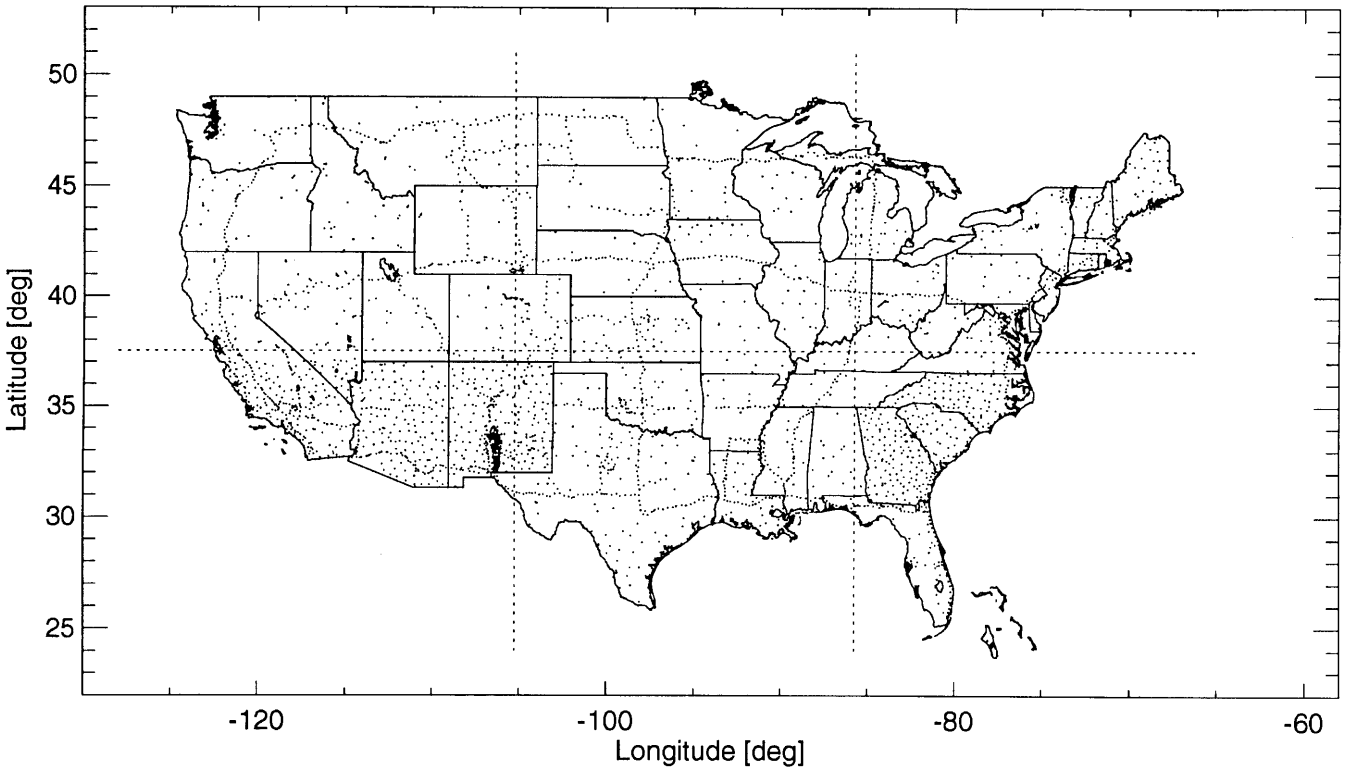

Fig. 3. Locations of 3561 astronomic deflections of the vertical

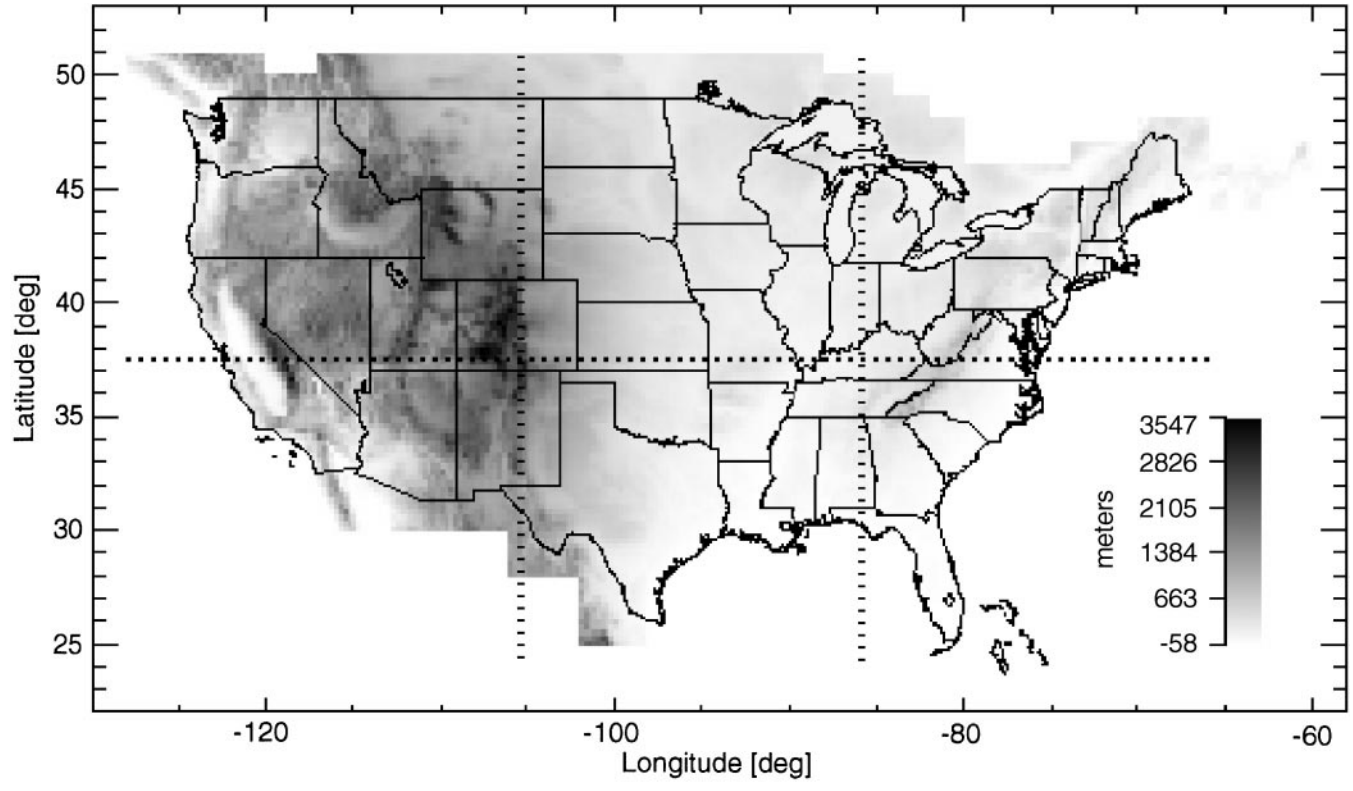

Fig. 4. Delineation of six area of CONUS, roughly by type of terrain

Table 2. Essential statistics of the astronomic and model-implied deflections of the vertical

		Region																	
		Northwest (489 pts)			North-central (468 pts)			Northeast (405 pts)			Southwest (1081 pts)			South-central (618 pts)			Southeast (500 pts)		
		Θ''	ξ''	η''	Θ''	ξ''	η''	Θ''	ξ''	η''	Θ''	ξ''	η''	Θ''	ξ''	η''	Θ''	ξ''	η''
Maximum	astro	31.62	18.04	31.04	24.73	10.87	24.73	15.52	8.43	12.11	32.29	20.19	26.36	19.82	19.78	10.72	16.41	11.31	11.37
	OSU91A	20.03	14.09	18.00	17.60	6.65	17.59	9.53	6.25	7.21	21.04	7.58	10.57	10.69	10.27	10.67	9.91	7.74	8.89
	EGM96	20.70	15.26	19.32	19.06	6.25	19.03	11.31	6.77	8.05	21.65	8.87	10.80	11.92	11.44	11.34	10.89	8.48	9.77
Minimum	astro	0.11	−13.42	−20.79	0.27	−15.81	−9.44	0.10	−10.58	−15.52	0.13	−25.83	−27.10	0.11	−10.31	−9.14	0.08	−12.77	−10.09
	OSU91A	0.40	−15.34	−12.88	0.15	−9.65	−4.49	0.25	−7.65	−9.45	0.25	−14.82	−16.47	0.15	−7.38	−7.72	0.15	−4.94	−6.16
	EGM96	0.21	−14.50	−14.12	0.04	−10.92	−5.55	0.29	−9.21	−11.11	0.27	−16.59	−17.41	0.08	−7.91	−8.42	0.19	−5.94	−6.23
Mean	astro		−0.63	−0.54		−0.36	3.24		+0.00	−0.45		−2.92	−2.91		0.44	0.74		0.20	2.26
	OSU91A		−1.02	−0.32		−0.39	3.32		−0.18	−0.52		−3.51	−3.46		0.46	0.91		0.33	2.61
	EGM96		−0.97	−0.26		−0.38	3.29		−0.13	−0.41		−3.48	−3.33		0.48	0.99		0.28	2.53
rms	astro	7.74	4.56	6.26	6.14	2.93	5.39	5.05	3.07	4.00	8.62	5.64	6.52	4.89	3.54	3.36	5.01	3.09	3.76
	OSU91A	5.80	3.67	4.49	5.35	2.37	4.80	3.89	2.26	3.16	6.78	4.52	5.05	4.23	3.00	2.99	4.39	2.37	3.68
	EGM96	6.25	3.88	4.90	5.66	2.55	5.05	4.28	2.65	3.37	6.98	4.70	5.15	4.55	3.19	3.24	4.54	2.46	3.77

Table 3. Essential statistics of the differences, model minus astronomic deflections

		Region																	
		Northwest (489 pts)			North-central (468 pts)			Northeast (405 pts)			Southwest (1081 pts)			South-central (618 pts)			Southeast (500 pts)		
		$\Delta\Theta''$	$\Delta\xi''$	$\Delta\eta''$	$\Delta\Theta''$	$\Delta\xi''$	$\Delta\eta''$	$\Delta\Theta''$	$\Delta\xi''$	$\Delta\eta''$	$\Delta\Theta''$	$\Delta\xi''$	$\Delta\eta''$	$\Delta\Theta''$	$\Delta\xi''$	$\Delta\eta''$	$\Delta\Theta''$	$\Delta\xi''$	$\Delta\eta''$
Maximum	OSU91A−astro	16.73	10.89	12.30	14.35	8.16	9.97	11.09	10.63	10.93	26.55	20.85	17.42	19.93	6.46	5.42	12.70	10.99	8.99
	EGM96−astro	16.24	11.29	14.00	13.08	8.29	9.57	11.30	10.67	9.92	25.76	20.63	16.88	19.62	6.42	6.84	10.22	9.53	8.24
Minimum	OSU91A−astro	0.08	−15.41	−16.59	0.11	−6.36	−14.21	0.06	−4.99	−8.41	0.19	−15.02	−21.27	0.10	−19.91	−3.98	0.10	−6.04	−7.23
	EGM96−astro	0.02	−14.25	−16.23	0.06	−6.20	−12.87	0.07	−5.01	−7.72	0.04	−14.37	−19.13	0.03	−19.57	−4.57	0.04	−5.65	−5.65
Mean	OSU91A−astro		−0.40	0.22		−0.03	0.09		−0.18	−0.07		−0.59	−0.56		0.02	0.17		0.13	0.35
	EGM96−astro		−0.35	0.28		−0.01	0.15		−0.14	0.04		−0.56	−0.42		0.04	0.25		0.08	0.28
rms	OSU91A−astro	5.28	3.33	4.10	2.67	1.73	2.04	2.50	1.68	1.85	6.34	4.02	4.90	2.25	1.78	1.37	2.33	1.72	1.57
	EGM96−zastro	5.20	3.30	4.01	2.63	1.71	2.00	2.42	1.62	1.80	6.14	4.00	4.67	2.19	1.69	1.38	2.18	1.59	1.49

errors in one or the other (or both) deflection types. These mean differences, however, do vary from one region to the next, being somewhat larger in the more mountainous areas. Table 4 gives the rms and mean deflections and differences between model and astronomic deflections for the entire CONUS as one region.

The theoretical differences between astronomic deflections and spherical harmonic model deflections are given by Eq. (35). Each of the calculable systematic correction terms in Eq. (35) is applied to the spherical harmonic model EGM96. The resulting corrected model deflections are then compared, again, to the astronomic deflections. Only the mean differences are computed since the rms, maximum and minimum differences will not differ substantively from the corresponding uncorrected differences. The term $(-\delta\xi_v)$ is computed from Eq. (30) using the gravity disturbance implied by EGM96. The combined term $(+\delta\xi_{\text{norm.curv}})$ is computed from Eq. (3) using the orthometric height plus geoid undulation implied by EGM96. The terms $(-\delta\xi_{\text{trans}})$ and $(-\delta\eta_{\text{trans}})$ are computed using Eq. (33) for the WGS84 to ITRF90 coordinate translations (McCarthy 1992)

$$\begin{aligned}\Delta x &= x_{\text{ITRF90}} - x_{\text{WGS84}} = -0.06\,\text{m}\\ \Delta y &= y_{\text{ITRF90}} - y_{\text{WGS84}} = +0.52\,\text{m}\\ \Delta z &= z_{\text{ITRF90}} - z_{\text{WGS84}} = +0.22\,\text{m}\end{aligned} \tag{37}$$

The terms $(-\delta\xi_{\text{rot}})$ and $(-\delta\eta_{\text{rot}})$ are computed using Eq. (34) for the WGS84 to ITRF90 coordinate rotations (McCarthy 1992)

$$\begin{aligned}\omega_x &= +0.0183\,\text{arcsec}\\ \omega_y &= -0.0003\,\text{arcsec}\\ \omega_z &= +0.0070\,\text{arcsec}\end{aligned} \tag{38}$$

It is assumed that the differences between ITRF90 and ITRF94 (to which EGM96 refers) are negligible. Finally, the term $(+\delta\xi^0_{\text{td}})$ is computed according to Eq. (22) and terms $(-\delta\xi_g)$ and $(-\delta\eta_g)$ are neglected (in accordance with the discussion of Table 1). Table 5 gives the mean effects of each of these corrections per region, as well as the total mean differences of the corrected and astronomic deflection components. The values that reduce these differences are highlighted in bold type, as are the corrected differences that show improvement. Corresponding rms values of these differences change insignificantly from the uncorrected differences.

Table 4. Essential statistics of the astronomic and model-implied vertical deflections and their differences

CONUS (3561 pts)	Mean value		rms value		
	ξ''	η''	Θ''	ξ''	η''
astro	−0.91	−0.14	6.79	4.27	5.28
OSU91A	−1.15	−0.19	5.46	3.42	4.26
EGM96	−1.13	−0.12	5.73	3.61	4.45
	$\Delta\xi''$	$\Delta\eta''$	$\Delta\Theta''$	$\Delta\xi''$	$\Delta\eta''$
OSU91−aastro	−0.24	−0.06	4.39	2.85	3.35
EGM96−astro	−0.22	0.02	4.27	2.81	3.22

Table 5. Mean effects of corrections terms and mean differences between corrected model and astronomic deflections

	Region											
	Northwest (489 pts)		North-central (468 pts)		Northeast (405 pts)		Southwest (1081 pts)		South-central (618 pts)		Southeast (500 pts)	
	$\Delta\xi''$ (mean)	$\Delta\eta''$ (mean)	$\Delta\xi''$ (mean)	$\Delta\eta''$ (mean)	$\Delta\xi''$ (mean)	$\Delta\eta''$ (mean)	$\Delta\xi''$(mean)	$\Delta\eta''$ (mean)	$\Delta\xi''$ (mean)	$\Delta\eta''$ (mean)	$\Delta\xi''$ (mean)	$\Delta\eta''$ (mean)
Correction												
$-\delta\xi_v$,	−0.0011		**0.0052**		**0.0060**		**0.0076**		0.0065		0.0035	
$+\delta\xi_{\text{norm.curv}}$	**0.217**		0.110		**0.039**		**0.157**		0.076		0.016	
$+\delta\xi^0_{\text{td}}$	**0.012**		0.012		**0.012**		**0.011**		0.011		0.011	
$-\delta\xi_{\text{trans}}$, $-\delta\eta_{\text{trans}}$	**0.015**	**−0.0087**	**0.016**	**−0.0039**	**0.016**	0.0018	**0.014**	−0.0083	0.015	**−0.0038**	0.015	0.0006
$-\delta\xi_{\text{rot}}$, $-\delta\eta_{\text{rot}}$	**0.017**	**−0.010**	0.018	**−0.0064**	**0.018**	**−0.0023**	**0.017**	−0.0097	0.018	**−0.0068**	0.018	**−0.0043**
mean (EGM96−astro)												
no corrections	−0.345	0.276	−0.014	0.152	−0.135	0.041	−0.564	−0.424	0.036	0.248	0.078	0.277
all corrections	**−0.082**	**0.257**	+0.148	**0.141**	**−0.044**	**0.041**	**−0.357**	−0.441	0.163	**0.237**	0.141	**0.274**

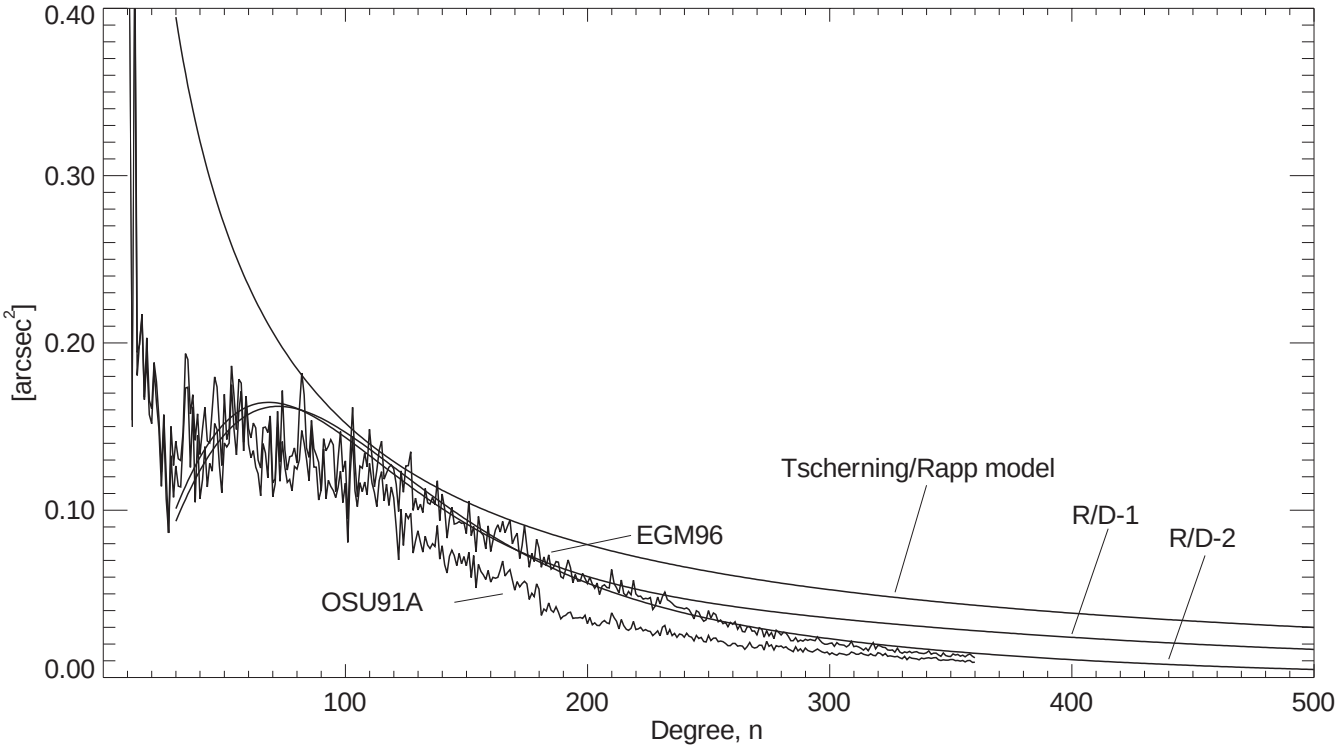

Fig. 5. Degree variances for the vertical deflection from spherical harmonic models EGM96 and OSU91A, as well as from analytical approximations

For the entire region, CONUS, the mean difference for the south–north deflection component was reduced, as a consequence of applying the systematic corrections, from $-\mathbf{0.219}$ arcsec to $\mathbf{-0.058}$ arcsec; and for the west–east component, it was reduced from $+\mathbf{0.016}$ arcsec to $+\mathbf{0.004}$ arcsec.

From Table 1, the largest differences between the model and astronomic deflections are caused by the truncation of the spherical harmonic series. Neglecting all systematic errors in Eq. (35), one has

$$\begin{aligned}\hat{\xi}^{\mathrm{grav}}_{\mathrm{tide-free}}(P) - \hat{\xi}^{\mathrm{astro}}(P) &\approx \delta\xi_{\mathrm{trunc}} + \delta\xi_{\mathrm{coeff.err}} + \delta\xi_{\mathrm{astro.err}} \\ \hat{\eta}^{\mathrm{grav}}(P) - \hat{\eta}^{\mathrm{astro}}(P) &\approx \delta\eta_{\mathrm{trunc}} + \delta\eta_{\mathrm{coeff.err}} + \delta\eta_{\mathrm{astro.err}}\end{aligned} \quad (39)$$

In terms of variances, one may assume that the errors on the right side are uncorrelated and obtain an approximate expression of the error variance for the deflection vector. In order to work with a single number, let

$$\begin{aligned}\sigma^2_{\Theta} &\equiv \mathrm{tr}\,\mathscr{M}(\boldsymbol{\Theta}\boldsymbol{\Theta}^{\mathrm{T}}) \\ &= \sigma^2_{\xi} + \sigma^2_{\eta}\end{aligned} \quad (40)$$

where $\mathscr{M}(\cdot)$ represents a global average or statistical expectation, as the case may be; and zero mean values are assumed. Then, from Eq. (39)

$$\sigma^2_{\Theta,\mathrm{tot}} \approx \sigma^2_{\Theta,\mathrm{trunc}} + \sigma^2_{\Theta,\mathrm{coeff.err}} + \sigma^2_{\Theta,\mathrm{astro.err}} \quad (41)$$

For EGM96, $\sigma^2_{\Theta,\mathrm{coeff.err}} = (1.80\,\mathrm{arcsec})^2$, and for the 3561 astronomic deflections, the rms of the error variances is $\sigma^2_{\Theta,\mathrm{astro.err}} = (0.49\,\mathrm{arcsec})^2$. Therefore, using the entry in the last row of Table 4, a reasonable estimate of the truncation error variance for CONUS is

$$\begin{aligned}\hat{\sigma}^2_{\Theta,\mathrm{trunc}} &= (4.27)^2 - (1.80)^2 - (0.49)^2 \\ &= (3.84\,\mathrm{arcsec})^2\end{aligned} \quad (42)$$

With a view toward evaluating this empirical value of $\sigma^2_{\Theta,\mathrm{trunc}}$, Fig. 5 shows the degree variances of the deflection vector, in the sense of Eq. (40), given by

$$\sigma^2_{\Theta,n} = n(n+1)\sum_{m=-n}^{n} C^2_{n,m} \quad (43)$$

for the OSU91A and EGM96 models, where the units of radians-squared in Eq. (43) are converted to arcseconds-squared in the figure. Also included in this figure are putative analytic approximations and continuations for the high degrees. They are based on the Tscherning/Rapp degree variance model (included for comparison; Tscherning and Rapp 1974)

$$\begin{aligned}&\sigma^2_{\Theta,n}(T/R) \\ &\quad = \frac{1}{\gamma^2}\frac{425.28\,n(n+1)}{(n-1)\,(n-2)\,(n+24)}\,(0.999617)^{n+2}\ [\mathrm{rad}^2]\end{aligned} \quad (44)$$

where $\gamma = 9.8 \times 10^5$, and a linear combination of spherical reciprocal distance (R/D) models

$$\sigma^2_{\Theta,n}(R/D) = \frac{n(n+1)}{\gamma^2 R^2} \sum_{j=1}^{p} s_j^2 (1-\rho_j)\,\rho_j^n \ [\mathrm{rad}^2] \qquad (45)$$

where $R = 6\ 371\ 000$ and s_j^2 is given in units of $[m^2/s^2]$. The parameter values given in Table 6 pertain to the R/D models shown in Fig. 5.

These parameter values are purely empirical based on the following criteria. Both R/D model degree variances should approximate the EGM96 degree variances from degree 100 to degree 200. R/D-1 model degree variances should yield the estimated truncation standard error given in Eq. (42). R/D-2 model degree variances should approximate EGM96 degree variances from degree 100 to degree $n_{\max} = 360$.

Table 7 compares the truncation errors implied by the degree variance models to the empirical truncation error for CONUS derived from a comparison of astronomic and EGM96 deflections. It is clear that this latter truncation error, given by Eq. (42), is consistent only with an analytic degree variance model that cannot fit the observed degree variances at degrees greater than 200. This means that the high-degree spectrum (greater than degree 200) of the EGM96 model has less power than the deflection data would suggest. A note of caution must accompany this conclusion, since it is based on only a relatively small part of the globe. For example, the rms deflection from the EGM96 degree variances is 6.57 arcsec, whereas for CONUS, from Table 4, it is 5.73 arcsec (but this would imply an rms truncation error even smaller than 1.33 arcsec in Table 7). Moreover, the distribution of astronomic deflections on which the analysis is based is not uniform even in this small part (namely, CONUS). Nevertheless, this analysis represents an evaluation of the EGM96 model against data that have strong high-frequency informational content and that are representative of a variety of signal strengths of the anomalous gravity field.

Table 6. Parameter values for the R/D models

Model	s_j^2 $[m^2/s^2]$	ρ_j
R/D-1, $p = 4$	0.4	0.99875
	5	0.9962
	70	0.989
	780	0.969
R/D-2, $p = 3$	60	0.988
	80	0.978
	650	0.970

Table 7. Standard errors of truncation for different models and CONUS [units = arcsec]

Model	Empirical (CONUS)	T/R model	R/D-1	R/D-2
$\sigma_{\Theta,\mathrm{trunc}}$	3.84	5.32	3.85	1.33

8 Summary

A careful theoretical development of the differences between astronomic vertical deflections and deflections implied by 360-degree spherical harmonic models shows that several systematic differences are significant at the level of a few hundredths of an arcsecond, or more. By far the largest difference is the effect due to the curvature of the normal plumb line. Accounting for this and other calculable systematic differences due to the permanent tide and datum translation and rotation reduces the *mean* differences between these two types of deflections in the conterminous US (CONUS) by about 75% , from -0.219 arcsec to -0.058 arsec and from $+0.016$ arcsec to $+0.004$ arsec, in their respective components. It is seen from Table 5 that the normal plumb-line curvature correction contributes most to the reduction of the mean differences in mountainous areas, as expected. This also reinforces the fact that large curvature corrections may need to be applied to gravimetric deflections computed at flight altitudes, if these are to be used in inertial navigation systems.

Since deflections of the vertical are rich in high-frequency gravitational information, observed values of the astronomic (or Helmert) deflections are well suited to assess the high-degree spectrum of a geopotential model like EGM96. Figure 5 clearly shows the improvement of EGM96 over OSU91A in the power of the signal at degrees greater than 100. However, when comparing EGM96 deflections with astronomic deflections in CONUS, the EGM96 deflections appear to be too smooth at degrees greater than 200. This conclusion is obtained by trying to fit, without success, models of the power remaining in the observed deflections after EGM96 is removed to that suggested by EGM96. It follows that the EGM96 model may be under-powered in the high-degree spectrum (say, beyond degree 200).

Acknowledgments. This work was supported in part by Phillips Laboratory, US Air Force, contract F19628-94-K-0005, and National Imagery and Mapping Agency. The author is grateful to NIMA for providing the astronomic deflection data and to Mr. Jian Yi, graduate student at Ohio State University, for performing some of the computations. The author also thanks the referees for their reviews.

References

Britting KR (1971) Inertial navigation systems analysis. John Wiley, New York

Cartwright DE, Tayler RJ (1971) New computations of the tide-generating potential. Geophys J R Astr Soc 23: 45–74

Heikkinen M (1978) On the tide-generating forces. Pub Finnish Geodetic Inst No 85, Helsinki

Heiskanen WA, Moritz H (1967) Physical geodesy. Freeman, San Francisco

Lambeck K (1988) Geophysical geodesy, the slow deformations of the Earth. Clarendon Press, Oxford

Lemoine FG, Smith DE, Kunz L, Smith R, Pavlis EC, Pavlis NK, Klosko SM, Chinn DS, Torrence MH, Williamson RG, Cox CM, Rachlin KE, Wang YM, Kenyon SC, Salman R, Trimmer R, Rapp RH, Nerem RS (1996) The development of the NASA

GSFC and NIMA Joint Geopotential Model. Proc Int Symp Gravity, geoid, and marine geodesy (GRAGEOMAR 1996), University of Tokyo, 30 Sept–5 Oct

McCarthy DD (ed) (1992) IERS standards (1992). IERS Tech Note 13, Obsde Paris, Paris

Pick M, Picha J, Vyskocil V (1973) Theory of the Earth's gravity field. Elsevier, Amsterdam

Rapp RH (1983) Tidal gravity computations based on recommendations of the Standard Earth Tide Committee. Bull d'Info, Commiss Permanente des Marees Terrestres, Brussels No 89, pp 5814–5819

Rapp RH (1992) Geometric geodesy, part II. Dep Geodetic Science and Surveying, The Ohio State University, Columbus

Rapp RH, Pavlis NK (1990) The development and analysis of geopotential coefficient models to spherical harmonic degree 360 J Geophys Res 95 (B13): 21 885–21 911

Rapp RH, Wang YM, Pavlis NK (1991) The Ohio State 1991 geopotential and sea surface topography harmonic coefficient models. Rep No 410, Dep Geodetic Science, The Ohio State University, Columbus

Torge W (1991) Geodesy, 2nd edn. Walter de Gruyter, Berlin

Tscherning CC, Rapp RH (1974) Closed covariance expressions for gravity anomalies, geoid undulations and deflections of the vertical implied by anomaly degree variance models. Rep No. 208, Dep Geodetic Science, The Ohio State University, Columbus

Vanicek P (1980) Tidal corrections to geodetic quantities. NOAA Tech Rep NOS 83 NGS 14, National Oceanic and Atmospheric Administration, National Ocean Survey, Washington, DC